Journal of Naval Architecture and Marine Engineering
June, 2022
https://doi.org/10.3329/jname.v19i1.50863 *http://www.banglajol.info*

BUONGIORNO MODEL WITH BROWNIAN AND THERMOPHORETIC DIFFUSION FOR MHD CASSON NANOFLUID OVER AN INCLINED POROUS SURFACE

K.Veera Reddy[1], Kolli Vijaya[2], G.Venkata Ramana Reddy[3]

[1]Research Scholar, Department of Mathematics, Koneru Lakshmaiah Education Foundation, Vaddeswaram, India.-522502.
E-mail: veerareddymscmed@gmail.com
[2]Department of Mathematics, Geethanjali institute of science and technology, Gangavaram, Nellore, India.-524137.
E-mail:vijji.maths@gmail.com
[3]Department of Mathematics, Koneru Lakshmaiah Education Foundation, Vaddeswaram, India-522502.
E-mail: gvrr1976@gmail.com

Abstract:

The key goal of the study under concern is to test the effects of Brownian movement and thermophoresis dispersion on MHD Casson nanofluid limit layer stream over a nonlinear slanted permeable extending surface, with the impact of convective limits and warm radiation with synthetic response. Nonlinear ODEs are gotten from overseeing nonlinear PDEs by utilizing good comparability changes. The amounts related with building angles, for example, skin grating, Nusselt number and Sherwood number alongside different effects of material factors on the speed, temperature, and focus, are explained and explained with outlines. The numerical consequences of the current investigation are acquired through the Runge-Kutta Fehlberg strategy alongside shooting procedure and in a constraining sense are diminished to the distributed outcomes for a precision reason.

Keywords: Casson nanofluid, MHD, power law fluid, convective boundaries, radiation effect

NOMENCLATURE

e_{ij}	(i, j)th component of the rate of deformation rate	ρ_f	Density of the convectional fluid, kg m^{-3}
μ_B	Plastic dynamic viscosity	ρ_p	Density of the Nanoparticle, kg m^{-3}
P_y	Yield stress of the fluid	β	Casson fluid parameter
σ^*	Stephen Boltzmann coefficient	β_t	Thermal expansion factor
k^*	Mean absorption constant	β_c	Concentration expansion constant
T	Temperature, k^{-1}	K	Permeabilitym, m^2
T_∞	Free stream temperature, k^{-1}	D_B	Brownian dissemination factor, cm^{2}s^{-1}
u, v	Velocity in x, y directions, ms^{-1}	D_T	Thermophoresis dispersion factor,
g	Gravitational acceleration, ms^{-2}	K	Thermal conductivity
B_0	Strength of the magnetic field, Am^{-1}	K_r	Chemical reaction rate constant
σ	Electrical conductivity, sm^{-1}	$(\rho c)_p$	Heat capacity of Nanoparticles
μ	Viscosity of the fluid	$(\rho c)_f$	Heat capacity of convectional liquid
		λ	Buoyancy parameter

1813-8535 (Print), 2070-8998 (Online) Received on: Dec., 2020

δ	Solutal buoyancy parameter	N_t	Thermophoresis factor
M	Magnetic constraint	N	Radiation factor
K_x	Permeability parameter	K_{r_x}	Chemical reaction parameter
υ	Kinematic viscosity, m^2s^{-1}	Cf	Skin friction
P_r	Prandtl number	Sh	Sherwood number
L_e	Lewis number	Nu	Nusselt number
N_b	Brownian motion parameter		

1. Introduction

The study of non-Newtonian fluid has received attention from researchers', engineers and scientists because of its numerous applications such as production of food, annealing, etc. Also, there are several manufacturing processes in industries due to non-Newtonian fluids. They are biological fluids, lubricants, paints, polymeric suspensions etc. Several models such as pseudo plastic model, Ellis model, power law model, viscoelastic model etc has been examined with different rheological equations and solved numerically in literature. Due to their complexity alongside nonlinearity, rheological equations of different type have been used by authors in literature to describe non-Newtonian fluids. Casson fluid behavior is different from all other types of non-Newtonian fluids. It is a shear thinning liquid that have indefinite viscosity at zero shear rate and vice versa. Examples of fluid that portrays this type of behavior are orange juice, tooth paste, honey, tomato sauce, human blood and soup. In 2012, Hayat et al. critically examined Casson fluid behavior flowing in a stretchable surface. Maboob and Das in 2019 presented the influence of melting on the flow of MHD Casson fluid past a stretchable sheet in a penetrable medium. Kamran et al. (2017) elucidate Casson nanofluid MHD flow. They solved their flow equations using Keller box method. Falodun et al. (2018) pondered on MHD heat along with mass transport of Casson fluid flow. They numerically solved their model using spectral relaxation method. Shah et al. (2019) critically examined the model of Cattaneo-Christov for Casson ferrofluids over a stretchable sheet. Their flow equations were solved using homotopy analysis method. Sodium alginate is another type of Casson fluid that many researchers have of recent pondered on because of its applications in pharmaceuticals, textiles as well as cosmetics. Sodium alginate is highly viscous, it has solubility properties and very safe. It is a type of Casson nanofluid. This type of fluid helps to enhance the fluid thermal properties. Khan et al. (2018) explored Sodium alginate MHD Casson nanofluid through a penetrable medium. Alwawi et al. (2020) recently considered Sodium alginate MHD Casson nanofluid over a solid sphere. The recent study of Idowu and Falodun (2020) extensively discussed heat along with mass transport of MHD Casson nanofluid.

The study of nanofluid is seriously trending in recent years. It is mostly treated as mixture made of a base fluid together with nanoparticle. The nanofluid portrays a characteristic of a rise in thermal conductivity of the basic fluid. The major thing that interest researchers that have studied the behavior of nanofluid is because of its applications in engineering such as therapy, food processing, biological materials, photodynamic etc. The study of Choi (1995) first introduced nanofluid in his work. In another study of Buongiorno (2006), nano-particles alongside convective transport of nanofluids was extensively discussed. After the study of Choi (1995) and Buongiorno (2006), many authors have analyzed Buongiorno model in the presence of nanofluids. Ajam et al. (2018) elucidate MHD nanofluid flow induced by a stretchable and a penetrable surface by employing Buogiorno's model. Their flow equations were solved using analytical approach and they discovered that large Biot number enhances the heat transport coefficient. Reddy et al. (2019) examined MHD slip flow of Carreau nanofluid by considering chemical reaction along with Soret-Dufour mechanism. They solved their model using numerical method and concluded that increase in thermophoresis lead to increase in the Nusselt number. Jaradat et al. (2018) discussed two-mode coupled Burgers equation. Idowu and Falodun (2020) recently discussed MHD non-Newtonian nanofluid over a plate. They solved their equations numerically and concluded that the imposed magnetic field degenerate velocity profile. Gangaiah et al. (2019) examined the impact of thermal radiation on mixed convection MHD flow of Casson nanofluid. Rafique et al. (2019) elucidate Buongiorno model analysis together with Brownian and thermophoretic diffusion for Casson nanofluid. Lund et al. (2019) studied MHD

flow of micropolar nanofluid with buoyancy impact. The transformed ODE was solved numerically. They concluded that increase in Richadson number declines the micropolar nanofluid velocity.

Investigation of heat transport along with boundary layer flow over an inclined porous surface has importance in the production of paper, drawing of glass, hot rolling, plastic film, wire drawing etc. Alao et al. (2016) gives detailed explanation of a chemically reacting fluid with heat and mass transport effect. The study of Fagbade et al. (2018) extensively discussed heat transport analysis of viscoelastic fluid over a penetrable surface. Their equations were solved using spectral method. Analysis of Falodun and Fadugba (2017) was basically on impact of heat transport on unsteady MHD boundary layer flow. El-dable et al. (2017) explained heat along with mass transport of second grade fluid flow. Rehman and Nadeem (2013) explored heat transport analysis of boundary layer flow. They solved their flow model numerically using Keller box method. Heat transport of nanofluids is applicable in areas such as in science and technology. Heat transport enhancements in free convection flow of nanofluids have been investigated by Aman et al. (2017). Rashidi and Mohimanian (2010) discussed unsteady boundary layer flow along with heat transport because of a stretchable sheet. Motsa and Makukula (2017) elucidate boundary layer flow heat alongside mass transport because of a stretchable surface. Singh and Shweta (2013) discussed flow and heat transport of Maxwell fluid under the impact of variable thermo-physical parameters. Khidir and Sibanda (2012) solved MHD flow and heat transport from a rotating disk in a penetrable medium numerically. Idowu and Falodun (2019) studied Soret-Dufour impact on MHD heat and mass transport of Walter's-B viscoelastic fluid. The recent study of Ahmed et al. (2020) explains the mechanism of Soret-Dufour, MHD, heat and mass transport boundary layer flow.

The thermophoresis explains the migration of small particles towards degenerating thermal gradient. The particles are driven from hot surface towards cold surface. An example of such particle is dust. The phenomena that propel this particle is called thermophoretic velocity while the force on the driven particle is called thermophoretic force. The consideration of thermophoresis together with Brownian motion is trending in recent research of fluid dynamics because of its applications in science and engineering. The impacts of thermophoresis on unsteady Oldroyd-B nanofluid flow have been elucidated by Awad et al. (2015). Mallikarjuna et al. (2016) examined thermophoresis along with transpiration impact on Non-Darcy convective flow. They applied numerical method in their flow equations, and they discovered that thermophoretic velocity changes according to physical parameters variations. Shehzad et al. (2013) examined impact of thermophoresis along with Joule heating on Jeffrey radiative fluid flow. Falodun et al. (2018) elucidate MHD heat along with mass transport of Casson fluid flow in the presence of thermophoresis. Reddy et al. (2018) examined the combined effects of thermophoresis along with Brownian motion on unsteady MHD nanofluid flow.

M. Ali et al. (2021) explained the analysis of boundary layer Nano fluid flow over a stretching permeable wedge-shaped surface with magnetic effect. M. Ali et al. (2017) explained the Numerical analysis of heat and mass transfer along a stretching wedge surface. M. Ali et al. (2017) examined Magneto hydro dynamic boundary layer nano fluid flow and heat transfer over a stretching surface. M. Ali et al. (2017) elucidate the similarity solution of unsteady MHD boundary layer flow and heat transfer past a moving wedge in nano fluid using the Buongiorno model. M. Ali et al. (2016) studied the effect of chemical reaction and variable viscosity on free convection MHD radiating flow over an inclined plate bounded by porous medium. R. Nasrin and M.A. Alim (2011) explained the effects of variable thermal conductivity on the coupling of conduction and joule heating with MHD free convection flow along a vertical flat plate. R. Nasrin and M.A. Alim (2010) examined the combined effects of viscous dissipation and temperature dependent thermal conductivity on MHD free convection flow with conduction and joule heating along a vertical flat plate. R. Nasrin (2010) elucidates the MHD free convection flow along a vertical flat plate with thermal conductivity and viscosity depending on temperature.

The aim of the present study is to explore areas which have been neglected by researchers in previously published works. Motivated by the above literature, we hereby present in this paper Buongiorno model with Brownian and thermophoretic diffusion movement for MHD Casson nanofluid. The numerical results for velocity, concentration alongside temperature are presented with the aid of diagrams. The computational results for physical quantities of engineering interest are presented using table.

2. Formulation of the problem:

Consider a 2D incompressible Casson nanofluid flow over a nonlinear inclined porous stretching sheet slanted at γ, where $u_w(x) = ax^m$ is the extending speed and $u_\infty(x) = 0$ is the free stream speed, in which X is the coordinate slanted towards the extending sheet and a is the constant and Kr is the chemical reaction. The transverse magnetic field B_0 is taken as normal to the track of the flow. The effects of the thermophoresis and the Brownian motion are considered. The temperature T and the nanoparticle fraction C take the values T_w and C_w at the wall. The impact of the thermal radiation is incorporated with a convective heating procedure considered by the temperature T_f and heat exchange factor h_f, which is proportional to x^{-1}. Meanwhile, the encompassing structures for nanofluid temperature and mass divisions T_∞ and C_∞ are achieved as y keeps an eye on infinity, as displayed in Figure 1.

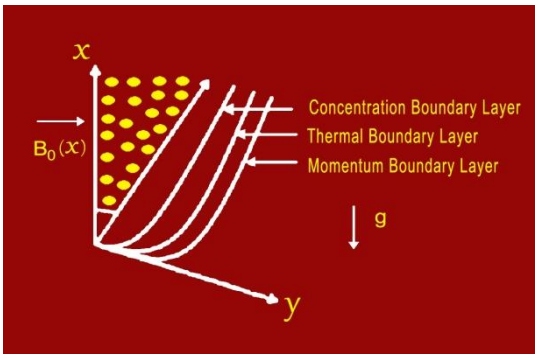

Figure 1: Physical model of the problem

The rheological model of state for an isotropic motion of a Casson liquid can be expressed as:

$$\tau_{ij} = \begin{cases} 2\left(\mu_B + \dfrac{P_y}{\sqrt{2\pi}}\right)e_{ij}, & \pi > \pi_c \\ 2\left(\mu_B + \dfrac{P_y}{\sqrt{2\pi_c}}\right)e_{ij}, & \pi < \pi_c \end{cases} \qquad (1)$$

In Equation (1) $\pi = e_{ij}e_{ij}$ where e_{ij} is the (i, j)[th] component of the rate of deformation rate. This implies that π signifies the product of the component of deformation rate with itself. Also, π_c signifies the critical value of this product according to the non-Newtonian model.

Casson fluid is a shear thinning liquid and assumed to have an infinite viscosity at zero rate of shear, a yield stress below no flow occurs and zero viscosity at an infinite rate of shear. If a shear stress less than the yield stress is applied to the Casson fluid it behaves like a solid where as if a shear stress greater than the yield stress is applied to the Casson fluid it starts to move.

Examples: Tomato Sauce, jellies, concentrated fruit juice, soup, honey, paints, synthetic lubricants, Human blood (which contains blood cell, chain structure and substances like protein, fibrinogen and rouleaux).

The Casson fluid model is used to describe the behavior of blood. Various experiment performed on blood with varying haematocrits, anticoagulants, temperatures, and the likes, strongly suggest the behaviour of blood as a Casson fluid.

The Casson fluid model is used in various fields like Biological fields, chemical fields, medical and engineering fields. petroleum drilling, polymer engineering, certain separation processes, and manufacturing of foods and paper.

The flow equations for this study are given by:

$$\frac{\partial u}{\partial x}+\frac{\partial v}{\partial y}=0 \quad (2)$$

$$u\frac{\partial u}{\partial x}+v\frac{\partial u}{\partial y}=\nu\left(1+\frac{1}{\beta}\right)\frac{\partial^2 u}{\partial y^2}+g\left[\beta_T\left(T-T_\infty\right)+\beta_C\left(C-C_\infty\right)\right]\cos\gamma-\frac{\sigma B_0^2\left(x\right)}{\rho}u-\frac{\nu}{K}u \quad (3)$$

$$u\frac{\partial T}{\partial x}+v\frac{\partial T}{\partial y}=\frac{\kappa}{\rho Cp}\frac{\partial^2 T}{\partial y^2}-\frac{1}{\left(\rho c\right)_f}\frac{\partial q_r}{\partial y}+\tau\left[D_B\frac{\partial C}{\partial y}\frac{\partial T}{\partial y}+\frac{D_T}{T_\infty}\left(\frac{\partial T}{\partial y}\right)^2\right] \quad (4)$$

$$u\frac{\partial C}{\partial x}+v\frac{\partial C}{\partial y}=D_B\frac{\partial^2 C}{\partial y^2}+\frac{D_T}{T_\infty}\frac{\partial^2 T}{\partial y^2}-K_r\left(C-C_\infty\right) \quad (5)$$

In this problem the boundary conditions are considered as:

$$u=u_w\left(x\right)=ax^m;\ v=0;\ -k\frac{\partial T}{\partial y}=h_f\left[T_f-T\right];\ C=C_w \text{ at } y=0$$
$$u\to u_\infty\left(x\right)=0;\ v\to o;\ T\to T_\infty;\ C\to C_\infty \text{ at } y\to\infty \quad (6)$$

The Roseland flux estimation is expressed as:

$$q_r=\frac{-4\sigma^*}{3k^*}\frac{\partial T^4}{\partial y} \quad (7)$$

Meanwhile, the changes in the temperature between the local temperature T and free stream T_∞ are very insignificant by ignoring the higher-order terms in the expansion of T^4 in Taylor succession about T_∞ for:

$$T^4=4T_\infty^3T-3T_\infty^4 \quad (8)$$

Using equations (7) and (8), the equation (4) is converted to:

$$u\frac{\partial T}{\partial x}+v\frac{\partial T}{\partial y}=\left[\alpha+\frac{16\sigma^*T_\infty^3}{3k^*\left(\rho c\right)_f}\right]\frac{\partial^2 T}{\partial y^2}-+\tau\left[D_B\frac{\partial C}{\partial y}\frac{\partial T}{\partial y}+\frac{D_T}{T_\infty}\left(\frac{\partial T}{\partial y}\right)^2\right] \quad (9)$$

where $\tau=\frac{\left(\rho c\right)_p}{\left(\rho c\right)_f}$ is the symbolic representation of the relation among the current heat capacity of the nanoparticle and the liquid.

For the conversion of the equations (3), (5) and (9) into ordinary differential equations, we use $\psi=\psi\left(x,y\right)$ known as the stream function, characterized as:

$$u=\frac{\partial\psi}{\partial y},v=-\frac{\partial\psi}{\partial x} \quad (10)$$

Introducing the similarity transformations as:

$$\psi=\sqrt{\frac{2\upsilon ax^{m+1}}{m+1}}f\left(\eta\right);\ \theta(\eta)=\frac{T-T_\infty}{T_w-T_\infty};\ \phi(\eta)=\frac{C-C_\infty}{C_w-C_\infty};\ \eta=y\sqrt{\frac{\left(m+1\right)ax^{m-1}}{2\upsilon}} \quad (11)$$

By using equations (10) and (11), the equation (2) is satisfied & the equations (3), (5) and (9) are transformed into the following ordinary differential equations:

$$\left(1+\frac{1}{\beta}\right)f'''+ff''-\frac{2m}{m+1}\left(f'\right)^2+\frac{2}{m+1}\left(\lambda\theta+\delta\phi\right)\cos\gamma-\frac{2}{m+1}\left(M+\frac{1}{K}\right)f'=0 \quad (12)$$

$$\frac{1}{\Pr}\left(1+\frac{4}{3}\mathrm{R}\right)\theta''+f\theta'+Nb\ \theta'\phi'+Nt\left(\theta'\right)^2=0 \quad (13)$$

$$\phi''+\left(Nt/Nb\right)\theta''+Lef\phi'-KrLe\phi=0 \quad (14)$$

The associated boundary conditions are transformed as:

$$f(\eta)=0;\quad f'(\eta)=1;\quad \theta'(0)=-Bi\left(1-\theta(0)\right);\quad \phi(\eta)=1 \text{ at } \eta=0$$
$$f'(\eta)\to 0;\qquad \theta(\eta)\to 0;\qquad \phi(\eta)\to 0 \text{ as } \eta\to\infty \tag{15}$$

The key parameters are as follows:

$$\lambda=\frac{Gr}{\mathrm{Re}_x^2};\quad \delta=\frac{Gc}{\mathrm{Re}_x^2};\quad M=\frac{\sigma B_0^2(x)x}{\rho u_w};\quad K=\frac{K_1 u_w}{\nu x},\ \mathrm{N}b=\frac{\tau D_B\left(C_w-C_\infty\right)}{\nu};$$
$$\mathrm{N}t=\frac{\tau D_T\left(T_w-T_\infty\right)}{\nu T_\infty};Gr=\frac{g\beta_T\left(T_w-T_\infty\right)x^3}{\nu^2};\quad Gc=\frac{g\beta_C\left(C_w-C_\infty\right)x^3}{\nu^2}; \tag{16}$$
$$Le=\frac{\nu}{D_B};\quad \mathrm{Pr}=\frac{\nu}{\alpha},R_{e_x}=\frac{u_w x}{\nu};\quad \mathrm{R}=\frac{4\sigma^* T_\infty^3}{k^* K};\quad Kr=\frac{2xK_r}{(m+1)u_w},Bi=\frac{\eta}{k\sqrt{\mathrm{Re}_x}}$$

The Skin friction, the Nusselt number and the Sherwood number for the current study are:

$$Cf=\frac{\tau_w}{u_w^2\rho f},\mathrm{N}u=\frac{xq_w}{k(T_w-T_\infty)};\ Sh=\frac{xq_m}{D_B(C_w-C_\infty)}; \tag{17}$$

Where $q_w=-\left[k+\frac{4\sigma^* T_\infty^3}{3k^*}\right]\frac{\partial T}{\partial y};q_m=-D_B\frac{\partial C}{\partial y};\ \tau_w=\mu\left(1+\frac{1}{\beta}\right)\frac{\partial u}{\partial y}$ at $y=0$

The related terms of the dimensionless reduced Nusselt number $-\theta'(0)$, the reduced Sherwood number $-\phi'(0)$ and the Skin friction coefficient $Cf=\left(1+\frac{1}{\beta}\right)f''(0)$ are defined as:

$$-\theta'(0)=\frac{\mathrm{N}u}{\left(1+\frac{4}{3}R\right)\sqrt{\left(\frac{m+1}{2}\right)\mathrm{Re}_x}};$$
$$-\phi'(0)=\frac{Sh}{\sqrt{\left(\frac{m+1}{2}\right)\mathrm{Re}_x}};Cf=Cf\sqrt{\left(\frac{m+1}{2}\right)\mathrm{Re}_x} \tag{18}$$

where $\mathrm{Re}_x=\frac{u_w x}{\upsilon}$ is the local Reynolds number.

3. Solution of the Problem

The governing boundary layer equations (12) through (14) subject to the boundary conditions of (15) are solved numerically by using the Runge-Kutta fourth-order method in conjunction with the shooting technique. First, the higher-order non-linear differential equations (12) through (14) have been converted into simultaneous linear differential equations of first-order and are further transformed into the initial value problem and it is solved numerically by applying the Runge-Kutta fourth-order along with the shooting technique. The Skin-friction, the Nusslet and the Sherwood numbers have been discussed in detail and various physical parameters have been illustrated graphically.

4. Results and Discussion

In this part of the study, the numerical outcomes of the converted nonlinear ordinary differential Equations (12)–(14) with boundary settings (15) are elucidated by the Runge-Kutta fourth-order method along with shooting technique. For the numerical results of physical parameters of our concern, namely, Brownian motion denoted by Nb, thermophoresis given by Nt, magnetic factor M, permeable parameter K, buoyancy factor λ, solutal buoyancy constraint δ,inclination factorα , Prandtl number Pr, Lewis number Le, radiation factor R, Casson fluid parameter β, chemical reaction parameter Kr Biot number *Bi* are shown graphically and tabular form.

The main aim of this study is base on the influence of Brownian movement along with thermophoresis on MHD Casson nanofluid limit layer over a nonlinear slanted permeable surface. The heat and mass transport problem was set up in the presence of thermal radiation, Brownian motion and thermophoresis. The flow model equations was solved numerically and physics of the problem is shown graphically. Also, we have computed

values for the physical quantities of engineering interest and shown using tables. Table 1 shows the behavior of pertinent flow parameters on local skin friction coefficient, Nusselt and Sherwood number. The results in table 1 show that all the flow parameters enhance the rate of heat and mass transport. This implies that there is a great enhancement in the hydrodynamic and thermal boundary layer thickness. This shows the usefulness of this research work in controlling the rate of cooling in heat transport.

Figure 2 represent the effect of magnetic parameter (M) and permeability parameter (K) on the velocity profile. The magnetic parameter (M) is noticed to decrease the velocity profile immediately its value is increased. M has great impact on the fluid flow such that when it is imposed transversely to fluid flow direction; it will produce a force called Lorentz force. In electromagnetism, Lorentz force is useful in engineering applications such as in plasma accelerators, MHD accelerator, hydrodynamic etc. Lorentz force is a phenomena that is responsible for slowing movement of an electrically conducting fluid. So, immediately the magnetic parameter increases more, it triggers the Lorentz force to decline the velocity as well as momentum boundary layer thickness. Also, increase in the permeability parameter (K) as shown in figure 2 enhances the velocity profile. The presence of K allows the transport of fluid particles from a region to another within the boundary layer. Now, increasing the value of K expands the hole and gives room for more movement of fluid particles.

Figure 3 shows the impact of the power index parameter (m) and the solutal buoyancy parameter (δ) on the velocity profile. The power index parameter (m) is noticed to enhance the velocity profile due to the presence of Brownian motion, thermophoresis along with Prandtl number. Hence, for large value of m, the velocity profile increases. The solutal buoyancy parameter (δ) is observed to increase the velocity profile in figure 3. Now, increase in (δ) lead to large solutal buoyancy force and reduction in the viscosity which leads to enhancement of the velocity profile. Figure 4 portrays the impact of thermal buoyancy parameter (λ) and Casson parameter (β) on the velocity profile. The buoyancy force parameter is noticed to increase the velocity profile as its value increases. Experimentally, increase in λ lead to reduction in the fluid viscosity which makes the fluid to thereby moves very fast. Therefore, increasing λ more lead to drastic increase in the velocity profile as shown in figure 4. Effect of β as shown in figure 4 is observed to decrease the velocity profile. This is true because β declines the yield stress in the Casson fluid. Hence, our experiment shows that β declines the yield stress meaning that plastic dynamic viscosity is improved and thereby makes the momentum boundary layer to become very thick. The imposed magnetic field strength transversely to the flow direction is also a reason while β degenerates the velocity profile. Figure 5 shows the impact of inclination factor (α) on velocity profile. Increase in α is noticed to degenerate the velocity profile. This is a reasonable result because the imposed magnetic field has all tendency of reducing the fluid movement and declines the velocity profile due to increase in α. In a moment $\alpha = 0$, it shows that maximum gravitational force acts on the flow. The velocity profile drops the more at $\alpha = \frac{\pi}{2}$.

Figure 6 depicts the effect of solutal buoyancy force parameter (λ) and Prandtl number (Pr) on the temperature profile. Increasing the value of α is noticed to decrease the temperature profile. The solutal buoyancy parameter acts like a pull which reduces the motion of an electrically conducting fluid because of the presence of M. also, increase in Pr is observed to reduces the temperature profile. Experimentally, the thermal conductivity of the fluid degenerates with increasing Pr. Hence, this lead to degeneration in the thermal boundary layer thickness. Figure 7 portrays the impact of radiation parameter (R) and Biot number (Bi) on the temperature profile. Thermal radiation shows great impact on heat transfer rate on the flow. Thermal radiation parameter helps to boast rate of heat transport. Hence, increase in R enhances the thermal condition of the fluid by increasing the temperature profile along with the thickness of thermal boundary layer. It is also observed in figure 7 that increase in Biot number boast the temperature. Hence, increase in the value of Bi means increase in heat transport coefficient. However, this increase in heat transport coefficient resulted to increase to increase in the fluid temperature.

Figure 8 portrays the impact of Brownian motion (Nb) and thermophoresis (Nt) on the temperature profile. Increasing the value of both Nb and Nt is observed to boast the temperature profile. This in return enhances the

rate of heat transport. This means that, the Brownian motion mechanism could be useful in distributing the nanoparticles in the flow regime. Also, small value of Nb and Nt could be useful in cooling of the flow regime. Figure 9 shows the impact of inclination factor (α) on the temperature profile. Increasing α is noticed to enhance the fluid temperature profile and the entire boundary layer thickness. Figure 10 depicts the impact of Nb and Nt on the concentration profile. Increase in the value of Nb is observed to degenerate the fluid concentration profile while increase in the value of Nt enhances the fluid concentration profile. This shows that, the thermophoresis parameter (Nt) helps the nanoparticle diffusion in the boundary layer. Also, the concentration boundary layer thickness becomes very low because of increase in the Brownian motion parameter (Nb). Figure 11 shows the effect of chemical reaction parameter (Kr) and Lewis number (Le) on the concentration profile. Lewis number is a dimensionless number which portrays the contribution of rate of thermal diffusion to rate of species diffusion. It is derived from the ratio of Schmidt number to Prandtl number. Therefore, when Le=1, heat alongside species diffuses at the same rate but when $Le > 1$, heat diffuses faster than species. Also, increase in the value of Kr is seen to be destructive on the concentration profile as increasing Kr degenerates the concentration profile. Figure 12 represents the effect of the inclination factor (α) on the concentration profile. A gradual increase in α is observed to give a slight increase to the concentration profile.

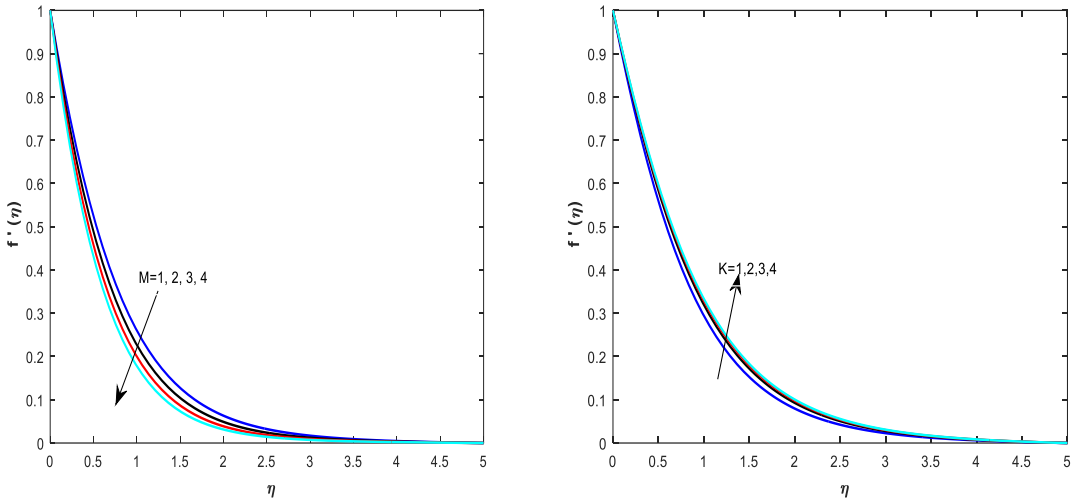

Figure 2: Effect of magnetic parameter (M) and permeability parameter (K) on velocity profile

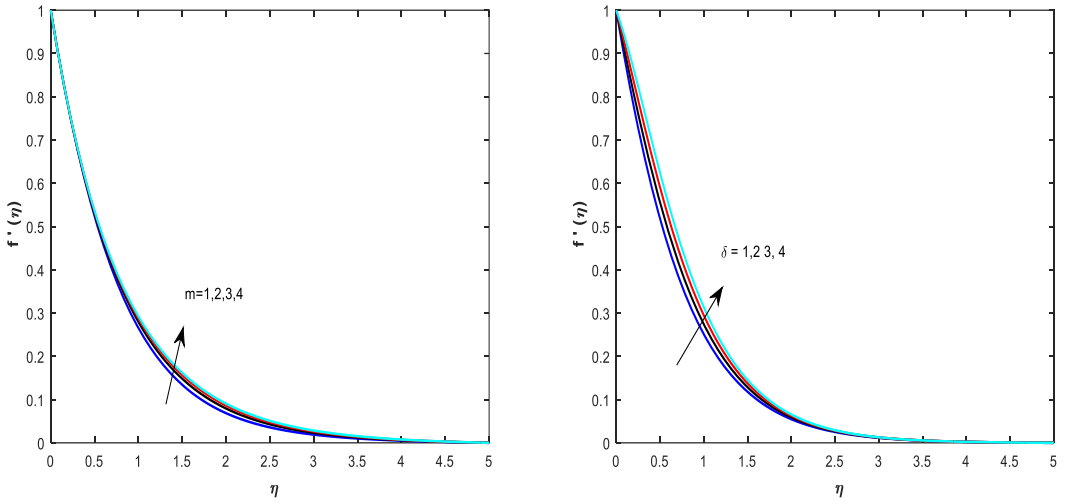

Figure 3: Effect of power index parameter (m) and solutal buoyancy parameter (δ) on velocity profile

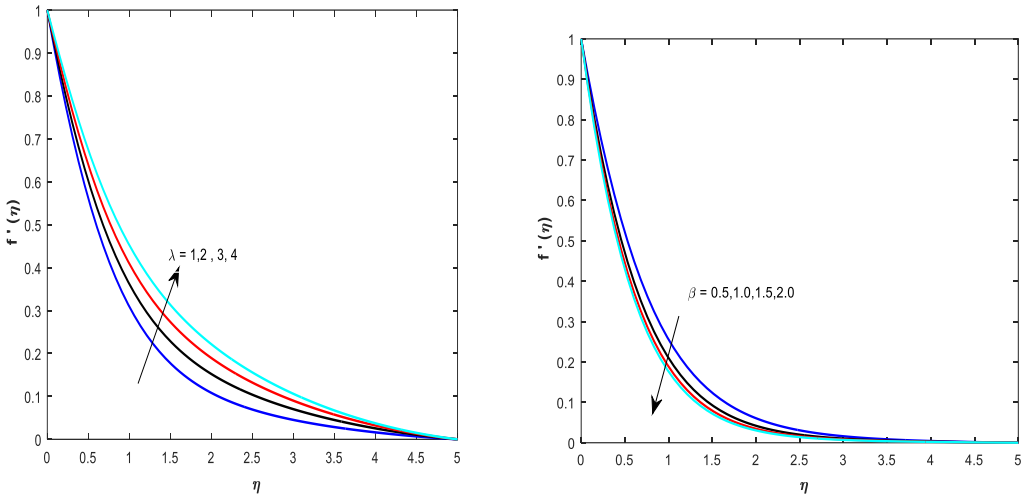

Figure 4: Effect of thermal buoyancy parameter (λ) and Casson parameter (β) on the velocity profile.

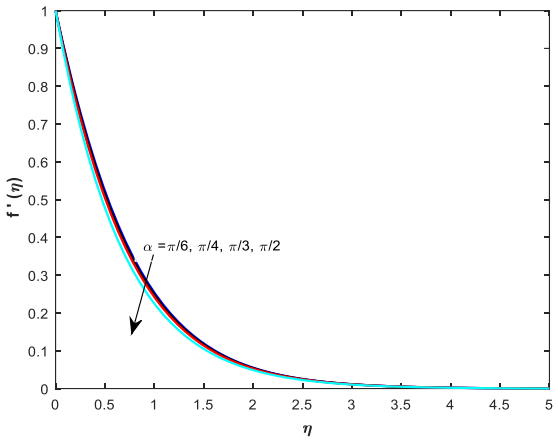

Figure 5: Effect of the inclination factor (α) on the velocity profile

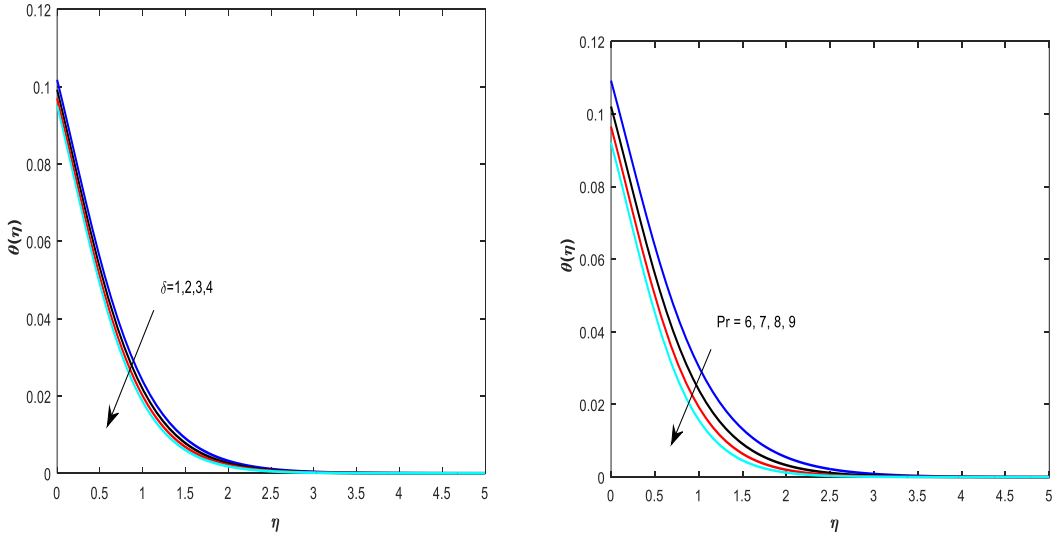

Figure 6: Effect of solutal buoyancy parameter (δ) and Prandtl number (Pr) on the concentration profiles

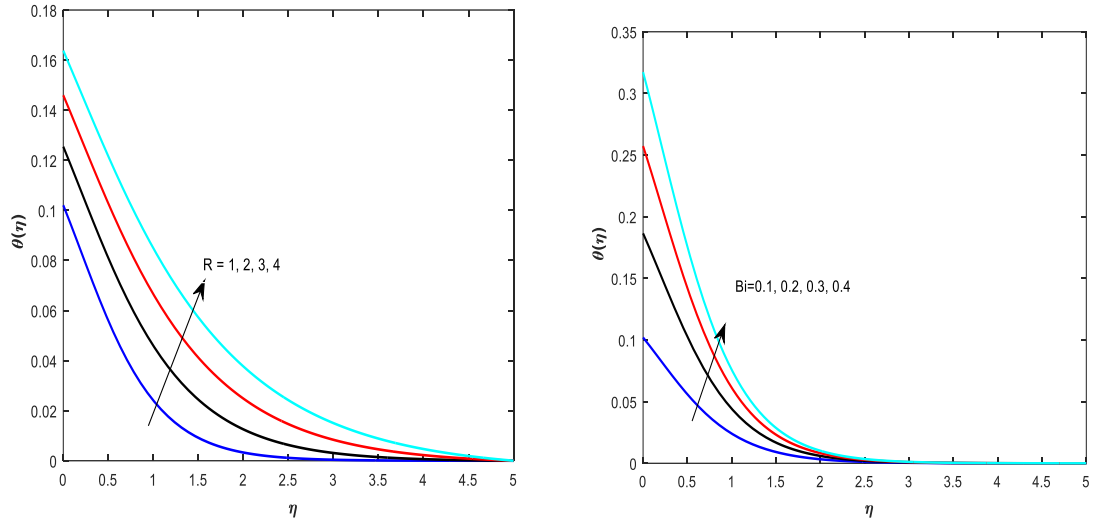

Figure 7: Effect of thermal radiation parameter (R) and Biot number (Bi) on the temperature profile

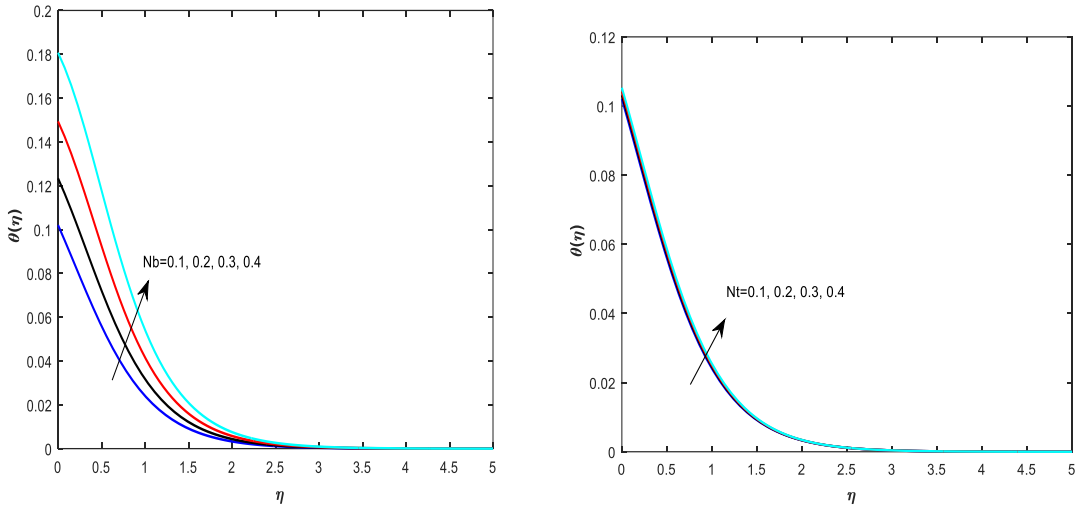

Figure 8: Effect of Brownian motion (Nb) and Thermophoresis parameter (Nt) on the temperature profile

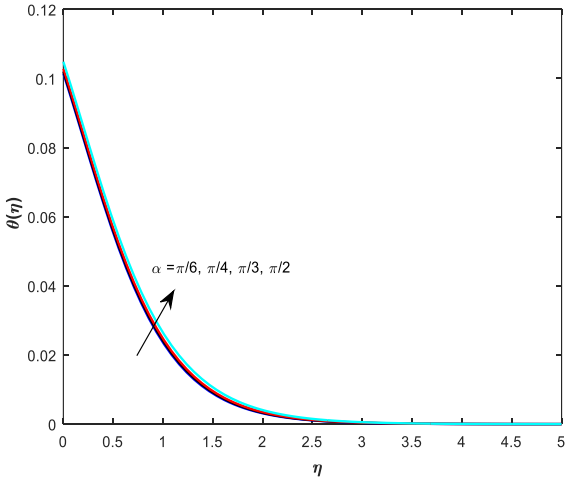

Figure 9: Effect of inclination factor (α) on the temperature factor

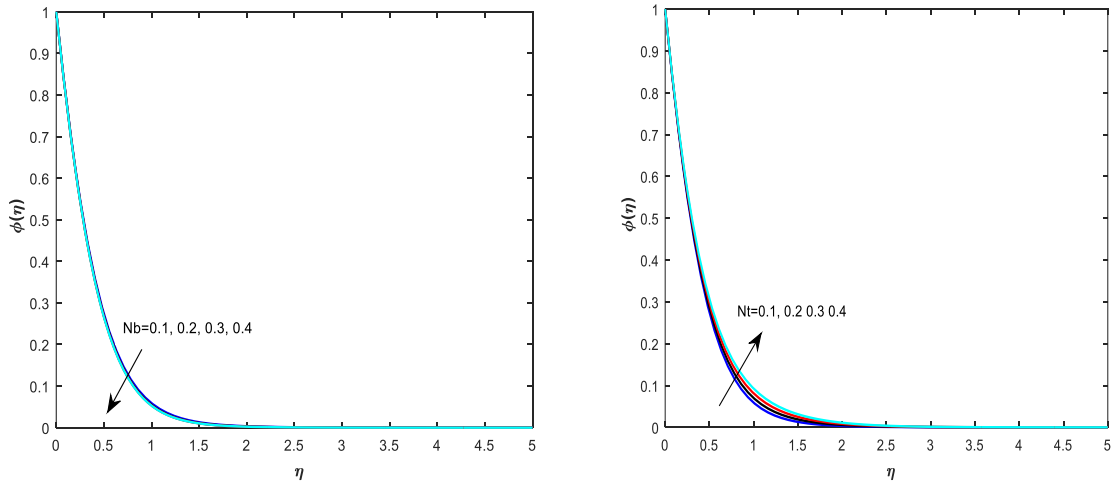

Figure 10: Effect of the Brownian motion (Nb) and Thermophoresis parameter (Nt) on the concentration profile

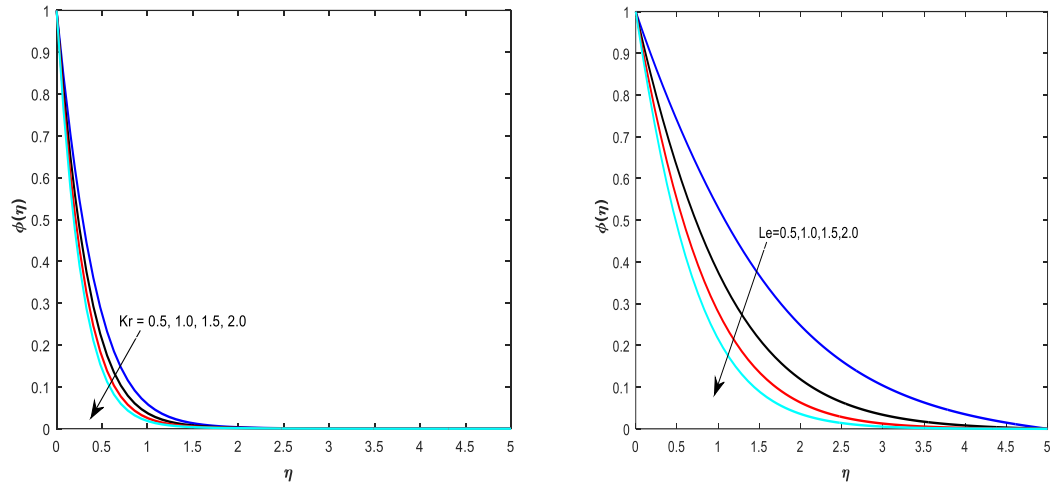

Figure 11: Effect of chemical reaction parameter (Kr) and Lewis number (Le) on the concentration profile

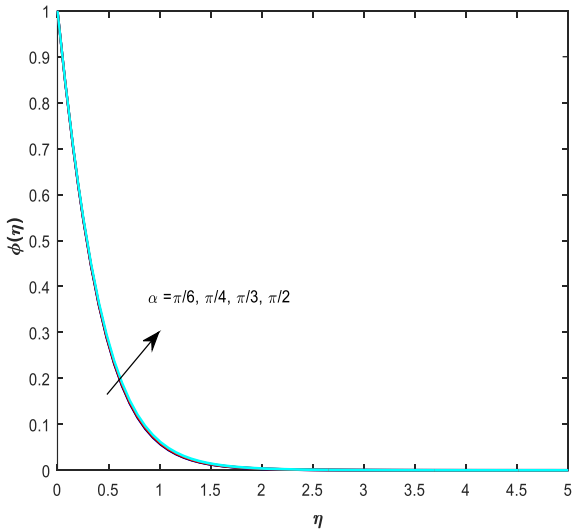

Figure 12: Effect of inclination factor (α) on the concentration profile

Table 1: Computational values of different flow parameters on local skin friction, Nusselt and Sherwood number.

M	K	M	λ	δ	β	Pr	R	Nb	Nt	Kr	Le	α	Bi	Cf	Nu	Sh
1	0.5	0.5	0.9	0.1	0.5	0.71	1	0.1	0.1	0.5	5	π/4	0.1	1.233354	0.072799	2.131724
2														1.383640	0.073107	2.144011
3														1.521480	0.073466	2.157612
4														1.649481	0.073892	2.172872
1	1	0.5	0.9	0.1	0.5	0.71	1	0.1	0.1	0.5	5	π/4	0.1	0.927143	0.074411	2.190304
	2													0.943393	0.074718	2.200075
	3													0.975295	0.074829	2.203521
	4													1.066662	0.074886	2.205283
1	0.5	1	0.9	0.1	0.5	0.71	1	0.1	0.1	0.5	5	π/4	0.1	1.248577	0.074017	2.174142
		2												1.262181	0.074168	2.175710
		3												1.268252	0.074254	2.176629
		4												1.271624	0.074311	2.177230
1	0.5	0.5	1	0.1	0.5	7	1	0.1	0.1	0.5	5	π/4	0.1	0.553403	0.089823	2.156779
			2											0.770516	0.090079	2.174759
			3											0.992048	0.090299	2.191762
			4											1.218581	0.090493	2.207915
1	0.5	0.5	1	1	0.5	0.71	1	0.1	0.1	0.5	5	π/4	0.1	0.729060	0.074638	2.190333
				2										0.841156	0.075284	2.205774
				3										0.959843	0.075825	2.219696
				4										1.086907	0.076291	2.232448
1	0.5	0.5	1	0.1	0.5	0.71	1	0.1	0.1	0.5	5	π/4	0.1	1.210731	0.072833	2.133445
					1									1.431945	0.073013	2.140694
					1.5									1.552122	0.073314	2.152397
					2									1.628086	0.073928	2.174682
1	0.5	0.5	0.9	0.1	0.5	6	1	0.1	0.1	0.5	5	π/4	0.1	1.241202	0.089083	2.153118
						7								1.241536	0.089796	2.153932
						8								1.241788	0.090348	2.154921
						9								1.241985	0.090789	2.156133
1	0.5	0.5	0.9	0.1	0.5	7	1	0.1	0.1	0.5	5	π/4	0.1	1.238474	0.083620	2.154921
							2							1.239388	0.085402	2.158643
							3							1.240417	0.087457	2.161399
							4							1.241536	0.089796	2.163519
1	0.5	0.5	0.9	0.1	0.5	7	1	0.1	0.1	0.5	5	π/4	0.1	1.241109	0.081929	2.154921
								0.2						1.241536	0.085064	2.171138
								0.3						1.242169	0.087661	2.177223
								0.4						1.242634	0.089796	2.180837
1	0.5	0.5	0.9	0.1	0.5	7	1	0.1	0.1	0.5	5	π/4	0.1	1.228234	0.089470	2.096771
									0.2					1.232675	0.089582	2.115110
									0.3					1.237109	0.089690	2.134505
									0.4					1.241536	0.089796	2.154921

1	0.5	0.5	0.9	0.1	0.5	7	1	0.1	0.1	0.5	5	π/4	0.1	1.241536	0.089434	2.154921
										1				1.264279	0.089517	2.678377
										1.5				1.280017	0.089630	3.115223
										2				1.291853	0.089796	3.497552
1	0.5	0.5	0.9	0.1	0.5	7	1	0.1	0.1	0.5	0.5	π/4	0.1	1.033845	0.090424	0.582769
											1			1.095579	0.090632	0.874960
											1.5			1.133928	0.090917	1.104605
											2			1.161051	0.091341	1.299896
1	0.5	0.5	0.9	0.1	0.5	7	1	0.1	0.1	0.5	5	π/6	0.1	1.194393	0.089515	2.137252
												π/4		1.241536	0.089718	2.149859
												π/3		1.303363	0.089796	2.154921
												π/2		1.454565	0.089853	2.158746
1	0.5	0.5	0.9	0.1	0.5	7	1	0.1	0.1	0.5	5	π/4	0.1	1.225173	0.089796	2.114918
													0.2	1.229707	0.162697	2.125481
													0.3	1.235082	0.222809	2.138521
													0.4	1.241536	0.273073	2.154921

5. Conclusions

The Runge-Kutta fourth-order method in conjunction with the shooting procedure has been utilized on the transformed differential equations (4.2.11) through (4.2.13) subject to (4.2.14), which describe the Buongiorno model with the Brownian and thermophoretic diffusion for the MHD Casson nanofluid flow with convective boundary conditions. The outcomes obtained in this study largely concur with those of the previously published works. The key findings in the present study are:

- A higher value of M is noticed to degenerate the velocity profile.
- The velocity profile degenerates with a larger value of β .
- The Biot number (Bi) is noticed to increase the heat transport coefficient.
- Higher values of Nb and Nt are observed to boost the temperature profile
- All the pertinent flow parameters have been noticed to enhance the rate of heat and mass transport by increasing the local Skin friction coefficient, the Nusselt and the Sherwood numbers.

References

Hayat, T. Shehzad, S.A. Alsaedi, A. and Alhothuali, M. S. (2012): Mixed convection stagnation point flow of Casson fluid with convective boundary conditions, Chin. Phys. Lett., Vol. 29,114704. https://doi.org/10.1088/0256-307X/29/11/114704

Mabood, F. and Kalidas, D. (2019): Outlining the impact of melting on MHD Casson fluid flow past a stretching sheet in a porous medium with radiation, Heliyon, Vol. 5. https://doi.org/10.1016/j.heliyon.2019.e01216

Kamran, S. Hussain, M. Sagheer, N. and Akmal, (2017): A numerical study of magnetohydrodynamics flow in Casson nanofluid combined with Joule heating and slip boundary conditions, Results in Physics, Vol. 7, pp. 3037-3048. https://doi.org/10.1016/j.rinp.2017.08.004

Falodun, B.O. Onwubuoya, C. and AwoniranAlamu F.H. (2018): Magnetohydrodynamics (MHD) Heat and Mass Transfer of Casson Fluid Flow Past a Semi-Infinite Vertical Plate with Thermophoresis Effect: Spectral Relaxation Analysis, Defect and Diffusion Forum, Vol. 389, pp 18-35. https://doi.org/10.4028/www.scientific.net/DDF.389.18

Zahir, S. Abdullah, D. Khan, I. Saeed, I. Dennis, L. C. C. Aurang, Z. and Khan (2019): Cattaneo-Christov model for electrical magnetite micropoler Casson ferrofluid over a stretching/shrinking sheet using effective thermal conductivity model, Case Studies in Thermal Engineering, Vol. 13. https://doi.org/10.1016/j.csite.2018.11.003

Arshad, K. Dolat, K, Ilyas, K. Farhad, A. Faizan, U. K. and Muhammad, I.(2018): MHD Flow of Sodium AlginateBased Casson Type Nanofuid Passing Through A Porous Medium With Newtonian Heating, SCIEnTIFICRePorTS, Vol. 8, pp. 1-12. https://doi.org/10.1038/s41598-018-26994-1

Firas, A. Alwawia, Hamzeh, T. Alkasasbeh, Rashad, A. M. and Ruwaidiah, I. (2020): MHD natural convection of Sodium Alginate Casson nanofluid over a solid sphere, Results in Physics, Vol. 16. https://doi.org/10.1016/j.rinp.2019.102818

Idowu, A. S. and Falodun, B.O. (2020): Effects of thermophoresis, Soret- Dufour on heat and mass transfer flow of magnetohydrodynamics non-Newtonian nanofluid over an inclined plate, Arab Journal of Basic and Applied Sciences, Vol. 27, pp. 149-165. https://doi.org/10.1080/25765299.2020.1746017

Hossein, A. SeyedSajad, J. Navid, F. (2018): Analytical approximation of MHD nano-fluid flow induced by a stretching permeable surface using Buongiorno's model, Ain Shams Engineering Journal, Vol. 9, pp. 525-536. https://doi.org/10.1016/j.asej.2016.03.006

Seethi Reddy, R. PoluBala, A. R. Ali, J. Ch.: Influence of Soret and Dufour effects on unsteady 3D MHD slip flow of Carreau nanofluid over a slandering stretchable sheet with chemical reaction, Nonlinear Analysis: Modelling and Control, Vol. 24, No. 6, 853-869. https://doi.org/10.15388/NA.2019.6.1

Jaradat, H. M. Muhammed, S. Marwan, A. Safwan, A. S. Khedr, M. Abohassn. (2018): A new two-mode coupled Burgers equation: Conditions for multiple kink solution and singular kink solution to exist, Ain Shams Engineering Journal, Vol. 9, pp. 3239-3244. https://doi.org/10.1016/j.asej.2017.12.005

Idowu, A. S. and Falodun, B.O. (2020): Effects of thermophoresis, Soret-Dufour on heat and mass transfer flow of magnetohydrodynamics non-Newtonian nanofluid over an inclined plate, Arab Journal of Basic and Applied Sciences, Vol. 27, pp. 149-165. https://doi.org/10.1080/25765299.2020.1746017

Gangaiah, T. Saidulu, N. and Venkata Lakshmi, A. (2019): The influence of thermal radiation on mixed convection MHD flow of a casson nanofluid over an exponentially stretching sheet, Int. J. Nanosci. Nanotechnol, Vol. 15, No. 2, pp. 83-98.

Khuram, R., Anwar, M. I., Misiran, M., Khan, I., Alharbi, S. O., Thounthong, P. and Nisar, K. S. (2019): Keller-box analysis of buongiorno model with Brownian and thermophoretic diffusion for casson nanofluid over an inclined surface, symmetry, Vol. 11. https://doi.org/10.3390/sym11111370

Liaquat, A. Zurni, O, and Ilyas, K. (2019): Mathematical analysis of magnetohydrodynamic (MHD) flow of micropolar nanofluid under buoyancy effects past a vertical shrinking surface: dual solutions, Heliyon, Vol. 5. https://doi.org/10.1016/j.heliyon.2019.e02432

Alao, A.I, Fagbade, A. I. and Falodun, B. O. (2016): Effects of thermal radiation, Soret and Dufour on an unsteady heat and mass transfer flow of a chemically reacting fluid past a semi-infinite vertical plate with viscous dissipation, Journal of the Nigerian Mathematical Society, Vol. 35, pp. 142-158. https://doi.org/10.1016/j.jnnms.2016.01.002

Fagbade, A. I. Falodun, B. O. and Omowaye, A. J. (2018): MHD natural convection flow of viscoelastic fluid over an accelerating permeable surface with thermal radiation and heat source or sink: Spectral Homotopy Analysis Approach, Ain Shams Engineering Journal, Vol. 9, pp.1029-1041. https://doi.org/10.1016/j.asej.2016.04.021

Falodun, B. O. and Fadugba, S. E. (2017): Effects of heat transfer on unsteady magnetohydrodynamics (MHD) boundary layer flow of an incompressible fluid a moving vertical plate, World Scientific News, Vol. 88, pp. 118-137.

Nabil, T. M. E. Refaie A. A. El-shekhipyand, A. A. Shalaby, G. A. (2017): Non-linear heat and mass transfer of second grade fluid flow with hall currents and thermophoresis effects, Appl. Math. Inf. Sci., Vol. 11, No. 1, pp. 267-280. https://doi.org/10.18576/amis/110133

Ahmad, S. Arifin, N. M. Nazar, R. Pop, I. (2008): Free convection boundary layer flow over cylinders of elliptic cross section with constant surface heat flux, Eur. J. Sci. Res., Vol. 23, No. 4, pp. 613-625.

Sidra, A. Ilyas, K. Zulkhibri, I. MohdZuki, S. and Qasem M. Al-Mdallal: Heat transfer enhancement in free convection flow of CNTs Maxwell nanofluids with four different types of molecular liquids, Scientific Reports 7: 2445. https://10.1038/s41598-017-01358-3

Rashidi, M.M. and Mohimanian Pour, S.A. (2010): Analytic approximate solutions for unsteady boundary-layer flow and heat transfer due to a stretching sheet by homotopy analysis method, Nonlinear Analysis: Modelling and Control, Vol. 15, No. 1, 83-95. https://doi.org/10.15388/NA.2010.15.1.14366

Motsa, S. S. and Zodwa, G. M. (2017): On a bivariate spectral homotopy analysis method for unsteady mixed convection boundary layer flow, heat, and mass transfer due to a stretching surface in a rotating fluid, Journal of Applied Mathematics Volume, Article ID 5962073, https://doi.org/10.1155/2017/5962073

Singh, V. Shweta, A. (2013): flow and heat transfer of Maxwell fluid with variable viscosity and thermal conductivity over an exponentially stretching sheet, American Journal of Fluid Dynamics, Vol. 3, No. 4, pp. 87-95. https://doi.org/10.5923/j.ajfd.20130304.01

Khidir, A. A and Sibanda, P (2012): On spectral-homotopy analysis solutions of steady magnetohydrodynamic (MHD) flow and heat transfer from a rotating disk in a porous medium, Scientific Research and Essays, Vol. 7, No. 31, pp. 2770-2780.

Idowu, A. S. and Falodun, B. O. (2019): Soret-Dufour effects on MHD heat and mass transfer of Walter's-B viscoelastic fluid over a semi-infinite vertical plate: spectral relaxation analysis, Journal of Taibah University for Science, Vol. 13, pp. 49-62. https://doi.org/10.1080/16583655.2018.1523527

Ahmed, L. O. Bidemi, O. F. JimohAbdul ,W.(2020): Mechanism of Soret-Dufour, magnetohydrodynamics, heat and mass transfer flow with buoyancy force, and viscous dissipation effects, Heat Transfer. pp. 1-18.

Awad, F. G. Ahamed, S. M. S. Sibanda, P. Khumalo, M. (2015): The effect of thermophoresis on unsteady Oldroyd-B nanofluid flow over stretching surface. PLoS ONE, Vol. 10. https://doi.org/10.1371/journal.pone.0135914

Mallikarjuna, B. Rashad, A. M. Ahmed Kadhim, H. Hariprasad Raju, S. (2016): Transpiration and thermophoresis effects on non-darcy convective flow past a rotating cone with thermal radiation, Arab J Sci Eng, Vol. 41, pp. 4691-4700. https://doi.org/10.1007/s13369-016-2252-x

Shehzad, S. A. Alsaedi, A and Hayat, T.: Influence of thermophoresis and joule heating on the radiative flow of jeffrey fluid with mixed convection, Brazilian Journal of Chemical Engineering, Vol. 30, No. 04, pp. 897 - 908. https://doi.org/10.1590/S0104-66322013000400021

Falodun, B. O., Onwubuoya, C. and AwoniranAlamu, F. H. Magnetohydrodynamics (MHD) heat and mass transfer of casson fluid flow past a semi-infinite vertical plate with thermophoresis effect: spectral relaxation analysis, Defect and Diffusion Forum, Vol. 389, pp 18-35. https://doi.org/10.4028/www.scientific.net/DDF.389.18

Reddy, J.V.R., Sugunamma, V. and Sandeep, N. (2018): Thermophoresis and Brownian motion effects on unsteady MHD nanofluid flow over a slandering stretching surface with slip effects, Alexandria Engineering Journa, Vol. 57, pp. 2465-2473. https://doi.org/10.1016/j.aej.2017.02.014

Ali, M. Nasrin, R. and Alim, M. A. (2021): Analysis of boundary layer Nano fluid flow over a stretching permeable wedge shaped surface with magnetic effect, Journal of Naval Architecture and Marin Engineering, Vol. 18, pp. 11-24. https://doi.org/10.3329/jname.v18i1.44458

Ali, M. Alim, M. A. Nasrin, R. and Alam, M. S. (2017): Numerical analysis of heat and mass transfer along a stretching wedge surface, Journal of Naval Architecture and Marin Engineering, Vol. 14, pp. 135-144 https://doi.org/10.3329/jname.v14i2.30633

Ali, M. Alim, M. A. Nasrin, R. Alam,M.S. and Chowdhury, M. Z. U. (2017): Magneto hydro dynamic boundary layer nano fluid flow and heat transfer over a stretching surface, AIP Conference Proceedings, Vol. 1851. https://doi.org/10.1063/1.4984651

Ali, M. Alim, M.A. Nasrin, R. Alam, and M. S. and Munshi, M.J.H. (2017): Similarity solution of unsteady MHD boundary layer flow and heat transfer past a moving wedge in nanofluid using the Buongiorno model, Procedia Engineering, Vol. 194, pp. 407-413. https://doi.org/10.1016/j.proeng.2017.08.164

Ali, M. Alim, M.A. Nasrin, R. and Alam, M. S. (2016): Study the effect of chemical reaction and variable viscosity on free convection MHD radiating flow over an inclined plate bounded by porous medium, The Journal of Chemical Physics, vol.1754. https://doi.org/10.1063/1.4958369

Nasrin, R and Alim, M. A. (2011): Effects of variable thermal conductivity on the coupling of conduction and joule heating with MHD free convection flow along a vertical flat plate, Journal of Naval Architecture and Marin Engineering, Vol. 7, No. 1. https://doi.org/10.3329/jname.v7i1.4322

Nasrin. R and Alim, M.A. (2010): Combined effects of viscous dissipation and temperature dependent thermal conductivity on MHD free convection flow with conduction and joule heating along a vertical flat plate, Journal of Naval Architecture and Marin Engineering, Vol. 6, No. 1. https://doi.org/10.3329/jname.v6i1.2648

Nasrin, R. (2010): MHD free convection flow along a vertical flat plate with thermal conductivity and viscosity depending on temperature, Journal of Naval Architecture and Marin Engineering, Vol. 6, No. 2. https://doi.org/10.3329/jname.v6i2.4994